Steel and Composite Structures, *Vol. 59, No. 2 (2026) 209-237*
https://doi.org/10.12989/scs.2026.59.2.209

Reliability analysis of steel frame structural systems via the generalized plastic hinge method and SVM approach

Da Lian Bai[a], Yan Xue Liao, Zhi Yi Wu, Jia Liang Wang*, Cun Peng Liu

College of Civil and Mapping Engineering, Guilin University of Technology at Nanning, Nanning, 530001, China

(Received February 16, 2026, Revised April 13, 2026, Accepted April 16, 2026)

Abstract. Steel frames are widely used because of their light weight, high ductility, and construction convenience. However, existing approaches for ultimate load-carrying capacity analysis struggle to balance accuracy and computational efficiency. The plastic-zone method provides high accuracy but low efficiency, whereas the conventional first-order plastic-hinge method is computationally efficient but neglects the influence of axial force on plastic hinge development, overestimating the structural ultimate load-carrying capacity. To address these issues, this study proposes a generalized plastic-hinge method based on a generalized yield criterion. An equivalent homogeneous yield function is introduced to construct an element-level load-carrying ratio, which captures the coupled effects of the axial force and bending moment on plastic hinge development while preserving proportional scaling with the external load. This formulation enables efficient and accurate evaluation of the ultimate load-carrying capacity. Subsequently, a small set of ultimate load-carrying capacity samples generated by the proposed method is used to reconstruct an explicit limit-state function via a support vector machine optimized by the particle swarm optimization for the reliability analysis. The numerical results demonstrate that the proposed method can accurately and reliably evaluate the structural ultimate load-carrying capacity. The reliability results obtained from the reconstructed limit-state function are in excellent agreement with those obtained from the Monte Carlo Simulation.

Keywords: steel frame structures; generalized plastic-hinge method; proportionality property; ultimate load-carrying capacity; support vector machine; reliability analysis

1. Introduction

Steel frame structures are widely used in the construction industry owing to their light weight, high ductility, and rapid construction. Current research commonly employs the ultimate load-carrying capacity of structures to guide design and reliability analysis, with two primary analytical approaches: the plastic-zone method and the plastic-hinge method [1, 2].

The plastic-zone method [3, 4] discretizes both the cross-section and member length in detail, enabling accurate simulation of material plasticity, residual stresses, and initial imperfections. However, this method suffers from low computational efficiency and is therefore mainly used as a benchmark or reference approach for validating other simplified analysis methods [5, 6].

The plastic-hinge method (PHM) [7-10] assumes that plasticity is concentrated at the element

*Corresponding author, Ph.D., Associate Professor, E-mail: WJL9812011@glut.edu.cn
[a] Ph.D., E-mail: baidl90@163.com

http://www.techno-press.org/scs/5 ISSN: 1229-9367 (Print), 1598-6233 (Online)

ends while the remaining portions remain elastic, allowing structural analysis with only a small number of elements and significantly improving computational efficiency. Among the various improved PHM, the refined plastic-hinge method (RPHM) [7, 10, 11] is the most widely used approach for ultimate load-carrying capacity analysis. Nevertheless, becauses the structural stiffness matrix in the RPHM includes unknown axial force terms, performing structural analysis requires nonlinear equation-solving techniques and extensive iterative procedures. Consequently, this approach entails a higher theoretical complexity and lower computational efficiency.

On the other hand, the traditional first-order plastic-hinge method (FPHM) [12, 13] divides the loading process into multiple steps based on the sequential formation of plastic hinges. By taking advantage of the proportional scaling relationship between the section linear-elastic bending moment and the external load, the traditional FPHM can efficiently identify the location of the newly formed plastic hinges and the corresponding external load increment.

The traditional FPHM enables efficient analysis of the structural ultimate load-carrying capacity and failure path, while maintaining theoretical simplicity and high computational efficiency. However, the traditional FPHM identifies plastic hinge formation based solely on the sectional bending moment and neglects the influence of the axial force. This omission leads to an overestimation of the ultimate load-carrying capacity of steel frame structures subjected to significant vertical loads [14, 15]. To incorporate the effect of the axial force, several studies [16-19] have employed generalized yield criteria involving both the axial force and bending moment to determine plastic hinge formation. Nevertheless, because these generalized yield criterias are typically nonlinear and non-homogeneous, the proportional scaling property of the traditional FPHM that underpins high efficiency cannot be preserved. Consequently, plastic hinge formation must be identified through incremental trial-and-error analysis, which substantially reduces the computational efficiency.

In structural reliability analysis, the first-order reliability method (FORM) [20-22] and second-order reliability method (SORM) [22-24] have been widely used. However, both methods rely on explicit performance function and are therefore not suitable for analyzing the implicit and highly nonlinear limit-state equations associated with the ultimate load-carrying capacity of steel frames. Although the Monte Carlo simulation (MCS) offers high accuracy, it requires an extremely large computational effort when dealing with small failure probabilities, making it difficult to satisfy engineering efficiency requirements.

Machine learning methods, including extreme gradient boosting (XGBoost) [25], random forest (RF) [25], artificial neural network (ANN) [26-28], and support vector machine (SVM) [29-31], have been widely adopted to construct input–output mappings of numerical models for implicit limit-state functions. Asgarkhani et al. [25, 32, 33] integrated numerical simulations with machine learning methods to efficiently evaluate seismic reliability and risk, providing a data-driven framework for structural reliability assessment. However, high-fidelity finite element analysis for steel frames is computationally expensive, which limits the generation of sufficient datasets for reliability analysis. Among various machine learning methods, the SVM is particularly effective for small-sample learning problems owing to its strong generalization capability and ability to reconstruct highly nonlinear implicit limit-state function [30, 31]. Moreover, it can be efficiently integrated with classical reliability methods such as the FORM and SORM to enable computationally efficient structural reliability analysis.

This study proposes a generalized plastic hinge method (GPHM) with proportional characteristics for an efficient ultimate load-carrying capacity analysis of steel frame structures, overcoming the limitations of the traditional FPHM. Furthermore, a SVM is employed to reconstruct explicit limit-state function for system reliability analysis. The remainder of this paper is organized as follows: Section 1 presents an introduction, reviewing the current state of research on the ultimate load-carrying capacity and reliability analysis of steel frame structures. Section 2 introduces the fundamental theory of the traditional first-order plastic hinge method, discusses its advantages and limitations, and presents the proposed GPHM. Section 3 develops an SVM-based explicit limit state function for structural system reliability analysis. Section 4 presents numerical examples to verify the accuracy and applicability of the proposed method. Finally, the main conclusions are summarized.

2. GPHM for ultimate load-carrying capacity analysis

2.1 Traditional FPHM

For an ideal elastic-plastic steel frame subjected to n external loads P_1, P_2, $\cdots$, P_n, the external load vector can be expressed as

$$\boldsymbol{P}=(P_1,P_2,\cdots,P_n)=F_0(\alpha_1,\alpha_2,\cdots,\alpha_n)=F_0\boldsymbol{\alpha}\,, \tag{1}$$

where $\boldsymbol{\alpha}=(\alpha_1,\alpha_2,\cdots,\alpha_n)$ denotes the vector of basic load ratios, and $P_k=F_0\alpha_k(k=1\sim n)$ represents the load component, with F_0 being the initial load multiplier. By incrementing the F_0, the proportional loading process of the structure can be simulated. For convenience of description in this paper, the load multiplier F_0 is used to represent the external load vector $\boldsymbol{P}$.

The traditional FPHM [12, 13, 34] divides the entire loading process into several steps based on the formation of plastic hinges. In this way, the nonlinear problem of ultimate load-carrying capacity analysis is transformed into a piecewise linear-elastic problem, enabling the rapid evaluation of the structural ultimate capacity with simple theory and high computational efficiency. Building on this framework, researchers worldwide have proposed various improvements and refinements of existing methods. The main analysis procedures are as follows:

1) Determination of the internal forces of each element. At the beginning of the i-th loading step, a linear elastic analysis is performed for the steel frame structure under the initial load F_0, and the sectional bending moment M_i^e of each element is obtained.

2) Determination of the normalized dimensionless bending moment. The normalized dimensionless bending moment m_i is calculated using Eq. (2), and the plastic yield level of the section is evaluated.

$$m_i=\frac{M_i^e}{M_{\mathrm{p},i}^e}\,, \tag{2}$$

where M_i^e is the bending moment at the beginning of the i-th loading step, in which the superscript e represents the element and the subscript i denotes the loading step. $M_{\mathrm{p},i}^e$ denotes the bending strength. When $i=1$, $M_{\mathrm{p},i}^e$ is taken as the initial bending strength of the section, that is

$M^e_{\mathrm{p},1} = F_\mathrm{y} Z$, where F_y is the material yield strength and Z is the plastic section modulus. When $i > 1$, the influence of the load effects accumulated in the previous loading steps on the current bending strength of the section should be considered, as follows:

(1) In the traditional FPHM, the bending strength of the section in the current loading step is corrected using the bending-moment increment $\bar{M}^e_{i-1}$ from the previous loading step [12], as expressed in Eq. (3).

$$M^e_{\mathrm{p},i} = M^e_{\mathrm{p},i-1} - \bar{M}^e_{i-1}, \tag{3}$$

where $\bar{M}^e_{i-1}$ denotes the increment in the bending moment at the i-1-th loading step.

(2) During the structural loading process, if the bending moment at a section changes sign between two adjacent loading steps, the corrected bending strength obtained from Eq. (3) may contain calculation errors. To address this issue, Wang [13] considered the effect of inconsistent directions between the bending-moment increment $\bar{M}^e_{i-1}$ in the previous step and the bending moment M^e_i in the current step, and proposed a modified calculation for the sectional bending strength, as given in Eq. (4).

$$M^e_{\mathrm{p},i} = M^e_{\mathrm{p},i-1} - \bar{M}^e_{i-1} \mathrm{sign}(\bar{M}^e_{i-1} \cdot M^e_i), \tag{4}$$

(3) However, the stepwise correction of the sectional bending strength adopted in Eq. (4) cannot accurately reflect the influence of the cumulative bending moment $M^e_{\mathrm{a},i}$ generated in the previous loading steps, which may lead to significant errors in some structures. Therefore, Yang and Yang [34] proposed computing the sectional bending strength using the cumulative bending moment $M^e_{\mathrm{a},i}$, together with the bending moment M^e_i in the current loading step, as shown in the following equation.

$$M^e_{\mathrm{p},i} = M^e_\mathrm{p} - M^e_{\mathrm{a},i}\ \mathrm{sign}(M^e_{\mathrm{a},i} \cdot M^e_i), \tag{5}$$

$$M^e_{a,i} = \sum_{k=1}^{i\text{-}1} \bar{M}^e_k, \tag{6}$$

During the structural linear elastic analysis, the normalized dimensionless bending moment m_i obtained from Eq. (2) varies proportionally with the external load F_0. When the maximum value of the normalized dimensionless bending moment in the structure reaches $m_i^{\max} = 1$, the corresponding section first attains its bending plastic strength and a plastic hinge forms at this location. At this moment, the location of $m_i^{\max}$ is identified as the position of the newly formed plastic hinge under the current loading step.

3) Determine the load and internal force increments. According to the proportional loading condition, the load increment $F_{\mathrm{L},i}$ and associated internal force increment under the current loading step are obtained as follows.

$$F_{\mathrm{L},i}=\frac{F_0}{m_i^{\max}},\ \bar{N}_i^e=\frac{N_i^e}{m_i^{\max}},\ \bar{M}_i^e=\frac{M_i^e}{m_i^{\max}}, \tag{7}$$

4) Determine the structural ultimate load-carrying capacity and failure path. After updating the stiffness matrix of the elements where the plastic hinges have formed, a new linear elastic finite element analysis is performed. This process continues until the structure transforms into a mechanism (that is, when the global stiffness matrix $\boldsymbol{K}_{i+1}$ becomes singular), at which point the structure reaches its ultimate load-carrying state and loading is terminated. During the loading process, the sequential formation of the plastic hinges constitutes a structural failure path. The ultimate load-carrying capacity F_{L} of the structure is obtained by summing the load increments $F_{\mathrm{L},i}$ of all the loading steps.

$$F_{\mathrm{L}}=\sum_{i=1}^{N_{\mathrm{L}}}F_{\mathrm{L},i}, \tag{8}$$

where N_{L} denotes the total number of loading steps.

Based on Eqs. (7) and (8), the traditional FPHM and its improved methods make use of the proportionality between the external load and normalized dimensionless bending moment. At each loading step, the external load increment required for the formation of a plastic hinge can be directly determined by scaling the initial load according to the maximum normalized dimensionless bending moment. The location corresponding to the maximum normalized dimensionless bending moment $m_i^{\max}$ indicates the position of the newly formed plastic hinge in the current loading step. By adopting the FPHM, the ultimate load-carrying capacity and failure path of the structure can be evaluated efficiently.

2.2 Proposed GPHM

2.2.1 Element load carrying ratio

The traditional FPHM and its improved methods determine the formation of plastic hinge based solely on a single sectional internal force, as expressed in Eq. (2). This approach fails to account for the combined effects of the bending moment and axial force on plastic hinge formation, and therefore inevitably leads to an overestimation of the ultimate load-carrying capacity of steel frame structures. To overcome this limitation, the present study employs a generalized yield criterion that captures the coupling interaction between the bending moment and axial force, enabling a more accurate identification of plastic hinge formation. Because steel frames predominantly use I-shaped section, this study adopts the McGuire yield criterion [35], which features both high accuracy and a concise mathematical form, and has been widely validated for welded I-sections and implemented in Mastan2 [36]. For other cross-sections (e.g., box section), the criterion proposed by Duan and Chen [37] may be adopted. The McGuire yield criterion is expressed as:

$$f=n_i^2+m_i^2+3.5n_i^2m_i^2=1, \tag{9}$$

where the normalized axial force n_i and bending moment m_i are defined as

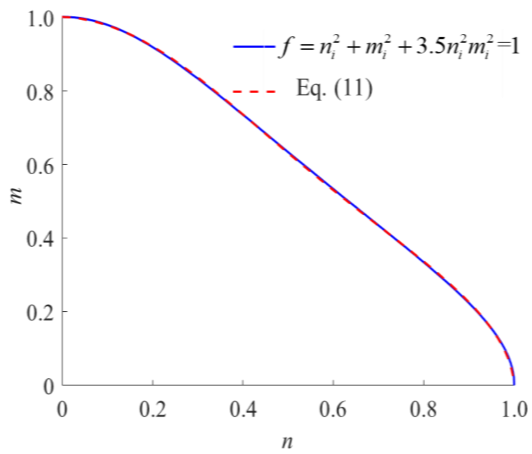

Figure 1 The generalized yield criterion

$$n_i = \frac{N_i^e}{N_{\mathrm{p},i}^e}\ ,\ \ m_i = \frac{M_i^e}{M_{\mathrm{p},i}^e}\ , \tag{10}$$

In this expression, N_i^e and M_i^e denote the linear elastic axial force and bending moment of section e under the initial load applied at the beginning of the current loading step, respectively. The terms $N_{\mathrm{p},i}^e$ and $M_{\mathrm{p},i}^e$ represent the corrected axial and bending strengths, respectively.

The generalized yield function f in Eq. (9) is a nonlinear and nonhomogeneous function of the normalized dimensionless axial force n_i and bending moment m_i. In the structural linear elastic analysis, although both n_i and m_i are proportional to the external load F_0, the yield function f itself does not satisfy the proportionality condition with respect to F_0 because of its inhomogeneous nature. Consequently, the direct application of f is incompatible with the load-proportional scaling required in the traditional FPHM. Therefore, it is necessary to homogenize f on the generalized yield surface so that the internal force terms have unified orders. An explicit functional expression with a consistent polynomial order is constructed via multivariate nonlinear regression to approximate the original generalized yield criterion f. The formulation procedure is detailed by Yang et al. [38], from which the equivalent homogeneous yield function $\overline{f}$ is obtained as follows:

$$\overline{f} = n_i^4 + 0.2122n_i^3m_i + 7.4536m_i^2n_i^2 + 0.1813m_i^3n_i + m_i^4\ , \tag{11}$$

A comparison between $\overline{f}$ and the original yield function f is presented in Fig. 1. The two yield surfaces exhibit identical geometrical shapes, indicating that the proposed $\overline{f}$ achieves a high level of accuracy in representing the original yield behavior. According to Eq. (11), the load-carrying ratio of element e is defined as:

$$r_i^e = \sqrt[4]{f} \,, \tag{12}$$

In structural linear elastic analysis, the external load F_0 is linearly proportional to the internal forces of the element. From Eq. (10), it is also known that the normalized dimensionless axial force n_i and bending moment m_i are linearly proportional to the internal forces of the element; therefore, both n_i and m_i remain linearly proportional to F_0. Furthermore, by combining Eqs. (11) and (12), it can be seen that the load-carrying ratio r_i^e is likewise linearly proportional to the external load F_0. Based on this important relationship, Eq. (2) can be replaced by Eq. (12) in the traditional FPHM to rapidly determine the plastic yielding degree of a section under a combined bending moment and axial force. When $r_i^e = 1$, the section fully reached the plastic limit state, and a plastic hinge is formed.

2.2.2 Section strength correction

During the structural loading process, the direction of the newly increased internal forces at the element ends significantly affects the sectional strength. If the direction is opposite to that of the previously accumulated internal forces, the accumulated internal forces resist part of the newly increased internal forces, thereby causing a strengthening effect on the section. If the direction is the same, the two jointly weaken the sectional strength. Therefore, it is necessary to dynamically correct the sectional strength under the current loading step by considering both accumulated internal forces and their combined effects. The corrected axial strength $N_{\mathrm{p},i}^e$ and bending strength $M_{\mathrm{p},i}^e$ of section *e* are given, respectively, as

$$N_{\mathrm{p},i}^e = N_\mathrm{p}^e \zeta_i^\mathrm{N} - N_{\mathrm{a},i}^e \,\mathrm{sign}(N_i^e \cdot N_{\mathrm{a},i}^e) \,, \tag{13}$$

$$M_{\mathrm{p},i}^e = M_\mathrm{p}^e \zeta_i^\mathrm{M} - M_{\mathrm{a},i}^e \,\mathrm{sign}(M_i^e \cdot M_{\mathrm{a},i}^e) \,, \tag{14}$$

$$N_{\mathrm{a},i}^e = \sum_{k=1}^{i\text{-}1} \bar{N}_k^e \,,\ M_{\mathrm{a},i}^e = \sum_{k=1}^{i\text{-}1} \bar{M}_k^e \,, \tag{15}$$

In these expressions, $N_{\mathrm{a},i}^e$ and $M_{\mathrm{a},i}^e$ represent the accumulated axial force and accumulated bending moment generated in section *e* during the previous loading steps, respectively. $\bar{N}_k^e$ and $\bar{M}_k^e$ denote the axial force and bending moment increments of section *e* in the *k*-th loading step. The initial axial strength N_p^e and bending strength M_p^e of section *e* are expressed as

$$N_\mathrm{p}^e = F_\mathrm{y} A \,,\ M_\mathrm{p}^e = F_\mathrm{y} Z \,, \tag{16}$$

where F_y denotes the material yield strength, A is the sectional area, and Z is the plastic section modulus.

In Eqs. (13) and (14), ζ_i^{N} and ζ_i^{M} represent the strength reduction factors that account for the influence of the accumulated axial force and bending moment on the sectional strength, corresponding to the axial strength and bending strength, respectively. In the first loading step (i = 1), the structure has no accumulated internal force, that is, $N_{\mathrm{a},1}^e = M_{\mathrm{a},1}^e = 0$. Therefore, there is no need to consider the correction of sectional strength, and it follows that the $\zeta_1^{\mathrm{N}} = \zeta_1^{\mathrm{M}} = 1$.

During the subsequent loading steps ($i > 1$), the sectional strength often depends on the combined effect of the accumulated bending moment $M_{\mathrm{a},i}^e$ and the accumulated axial force $N_{\mathrm{a},i}^e$. In this case, both ζ_i^{N} and ζ_i^{M} are less than 1. Based on the accumulated internal force and generalized yield criterion (Eq. (9)), the following expression is derived:

$$\zeta_i^{\mathrm{N}} = \sqrt{\frac{1 - m_{\mathrm{a},i}^2}{1 + 3.5 m_{\mathrm{a},i}^2}} \ , \ \zeta_i^{\mathrm{M}} = \sqrt{\frac{1 - n_{\mathrm{a},i}^2}{1 + 3.5 n_{\mathrm{a},i}^2}} \ , \tag{17}$$

$$n_{\mathrm{a},i} = \frac{N_{\mathrm{a},i}^e}{N_{\mathrm{p}}^e} \ , \ m_{\mathrm{a},i} = \frac{M_{\mathrm{a},i}^e}{M_{\mathrm{p}}^e} \ , \tag{18}$$

2.2.3 Overall calculation procedure

In linear elastic structural analysis, the element load-carrying ratio r_i^e, as defined in Eq. (12) maintains a proportional relationship with the external load F_0. During the loading process, all r_i^e increase proportionally with F_0, and loading proceeds until the maximum load-carrying ratio reaches $r_i^{\max} = 1$. At this stage, the corresponding section attains its plastic limit state, and the loading process for the current step is terminated. The location where $r_i^{\max}$ occurred is the position of the newly formed plastic hinge under the current loading step. According to the proportional relationship, the maximum load increment $F_{\mathrm{L},i}$ in the current loading step and the corresponding internal force increments $\bar{N}_i^e$ and $\bar{M}_i^e$ can be determined directly as follows:

$$F_{\mathrm{L},i} = \frac{F_0}{r_i^{\max}} \ , \bar{N}_i^e = \frac{N_i^e}{r_i^{\max}} \ , \bar{M}_i^e = \frac{M_i^e}{r_i^{\max}} \ , \tag{19}$$

Subsequently, the element at which the maximum load-carrying ratio $r_i^{\max}$ is attained is converted into a plastic hinge, and the global stiffness matrix of the structure is reconstructed to obtain $\boldsymbol{K}_{i+1}$. The singularity of $\boldsymbol{K}_{i+1}$ is then examined. If $\boldsymbol{K}_{i+1}$ remains non-singular, the next loading step is initiated, and a new linear elastic structural analysis is performed. Conversely, if $\boldsymbol{K}_{i+1}$ becomes singular, the structure transforms into a collapse mechanism and reaches its ultimate load-carrying state, at which point the loading process is terminated. During the loading procedure, the sequential formation of the plastic hinges constitutes a structural failure path. The ultimate load-carrying capacity F_{L} of the structure is obtained by summing the load increments $F_{\mathrm{L},i}$ over all loading steps, as follows:

$$F_{\mathrm{L}} = \sum_{i=1}^{N_{\mathrm{L}}} F_{\mathrm{L},i} \,, \tag{20}$$

where N_L denotes the total number of loading steps.

To address the inherent limitation of the traditional FPHM, in which the plastic hinge formation is determined solely by a single sectional internal force as expressed in Eq. (2), the present study adopts a homogenized formulation of the generalized yield criterion to define the element load-carrying ratio (Eq. (12)), which explicitly incorporates the combined effects of multiple sectional internal forces on plastic hinge formation. Based on the proportional relationship between the element load-carrying ratio and external load, the location of the newly formed plastic hinge and the corresponding external load increment at each loading step can be directly identified. Accordingly, the GPHM is developed to efficiently evaluate both the ultimate load-carrying capacity and failure path of steel frames.

3. Reliability analysis method for structural systems

3.1 Limit state function

By defining the structural response corresponding to the ultimate load-carrying capacity of the steel frame structures as the load effect S, and defining the structural ultimate load-carrying capacity as the resistance R, the limit-state function of the steel frame structures can be expressed as

$$G(\boldsymbol{X}) = R(\boldsymbol{X}) - S \,, \tag{21}$$

In the above equation, $\boldsymbol{X} = [X_1 \quad X_2 \quad \cdots \quad X_n]^{\mathrm{T}}$ denotes the vector of basic random variables influencing the ultimate load-carrying capacity of the structure, including the material properties, sectional geometric parameters, initial imperfections, and distribution of external loads. For steel frame structures subjected to complex loading conditions, the structural resistance $R(\boldsymbol{X})$ in Eq. (21) can only be evaluated through finite element analysis and cannot be expressed explicitly. Consequently, the limit-state function of the steel frame structure appears in an implicit form, which renders the conventional first-order and second-order reliability methods (FORM/SORM) inapplicable for reliability assessment.

3.2 SVM-based reconstruction of the limit-state function

Subsequently, the SVM approach is employed to reconstruct an approximate limit-state function to replace the implicit limit-state function in Eq. (21), thereby enabling a reliability analysis of steel frame structures. The SVM constructs an optimal decision function in a high-dimensional feature space, achieving an accurate approximation of complex nonlinear mappings between structural responses and random variables while maintaining good generalization performance. For the SVM with a linear ε-insensitive loss function, the model parameters are obtained by solving the following optimization problem:

$$\begin{cases} \min \dfrac{1}{2}\|\boldsymbol{\omega}\|^2 + C\sum_{i=1}^{m}(\xi_i + \xi_i^*) \\ s.t.\begin{cases} (\boldsymbol{\omega}\cdot \boldsymbol{x}_i + b) - y_i \le \varepsilon + \xi_i \\ y_i - (\boldsymbol{\omega}\cdot \boldsymbol{x}_i + b) \le \varepsilon + \xi_i^* \\ \xi_i,\ \xi_i^* \ge 0 \end{cases} \end{cases}, \tag{22}$$

where $\boldsymbol{x}_i$ denotes the i-th sample vector, expressed as $\boldsymbol{x}_i = [x_{i1} \quad x_{i1} \quad \cdots \quad x_{in}]^{\mathrm{T}}$, $i = 1,\ 2,\ \cdots,\ m$; y_i is the corresponding response value; ξ_i and ξ_i^* are slack variables; C is the penalty parameter; ε denotes the insensitive loss parameter; $\boldsymbol{\omega}$ and b are the parameters of the decision function. By introducing Lagrange multipliers and applying the Karush-Kuhn-Tucker optimality conditions, Eq. (22) can be transformed into the following dual formulation:

$$\begin{cases} \min \dfrac{1}{2}\sum_{i=1}^{m}(\alpha_i^* - \alpha_i)(\alpha_j^* - \alpha_j)(\boldsymbol{x}_i \cdot \boldsymbol{x}_j) + \varepsilon\sum_{i=1}^{m}(\alpha_i^* + \alpha_i) - \sum_{i=1}^{m} y_i(\alpha_i^* - \alpha_i) \\ s.t.\begin{cases} \sum_{i=1}^{m}(\alpha_i^* - \alpha_i) = 0 \\ 0 \le \alpha_i,\ \alpha_i^* \le C \end{cases} \end{cases}, \tag{23}$$

For complex practical engineering structures, the relationship between the structural responses and basic random variables is inherently nonlinear and cannot be accurately captured by linear regression models. Therefore, a nonlinear mapping function φ is required to map the sample points into a high-dimensional feature space, after which a linear SVM analysis can be performed. The corresponding optimization problem is formulated as

$$\begin{cases} \min \dfrac{1}{2}\sum_{i=1}^{m}(\alpha_i^* - \alpha_i)(\alpha_j^* - \alpha_j)k(\boldsymbol{x}_i \cdot \boldsymbol{x}_j) + \varepsilon\sum_{i=1}^{m}(\alpha_i^* + \alpha_i) - \sum_{i=1}^{m} y_i(\alpha_i^* - \alpha_i) \\ s.t.\begin{cases} \sum_{i=1}^{m}(\alpha_i^* - \alpha_i) = 0 \\ 0 \le \alpha_i,\ \alpha_i^* \le C \end{cases} \end{cases}, \tag{24}$$

where $k(\boldsymbol{x}_i \cdot \boldsymbol{x}_j)$ denotes the inner product of the mapped sample points in the high-dimensional feature space, defined as $k(\boldsymbol{x}_i \cdot \boldsymbol{x}_j) = \varphi(\boldsymbol{x}_i)\cdot\varphi(\boldsymbol{x}_j)$ and is referred to as the kernel function. Owing to its favorable statistical properties and effectiveness in modeling complex nonlinear relationships, the radial basis function (RBF) kernel is adopted and expressed as

$$k(\boldsymbol{x}\cdot \boldsymbol{x}_i) = \exp(-\gamma\|\boldsymbol{x} - \boldsymbol{x}_i\|^2), \tag{25}$$

Consequently, the SVM-based approximation of the limit-state function is obtained as:

$$f(\boldsymbol{x})=\sum_{i=1}^{m}(\alpha_i^*-\alpha_i)k(\boldsymbol{x}\cdot\boldsymbol{x}_i)+b\,, \tag{26}$$

3.3 Hyperparameter optimization

From Eqs. (24) and (25), the SVM-based reconstructed limit-state function depends on three key parameters, C , γ , and ε , which have a significant influence on model accuracy. Since manual tuning is inefficient, the particle swarm optimization (PSO) is adopted to globally optimize these parameters, enabling automatic identification of the optimal parameter combination and improving the predictive performance of the model.

The PSO [39-41] is a population-based global optimization algorithm. Candidate solutions are represented by particles that iteratively update their positions and velocities according to their individual best solutions and global best solution of the swarm. Through this mechanism, the PSO efficiently explores the search space and achieves a robust convergence toward the optimal solution.

In the PSO algorithm, the velocity and position of the *j*-th particle in the *d*-th dimension at the *k*-th iteration are updated according to Eqs. (27) and (28) [40].

$$v_{jd}^{k+1}=\omega\times v_{jd}^{k}+c_1\times r_1\times(p_{jd}^{k}-x_{jd}^{k})+c_2\times r_2\times(p_{gd}^{k}-x_{jd}^{k})\,, \tag{27}$$

$$x_{jd}^{k+1}=x_{jd}^{k}+v_{jd}^{k}\,, \tag{28}$$

where v_{jd} and x_{jd} denote the velocity and position of the particle, respectively; ω is the inertia weight; c_1 and c_2 are the acceleration coefficients; r_1 and r_2 are random numbers uniformly distributed in [0,1]; and p_{jd} and p_{gd} represent the historical personal best position of the particle and the global best position of the swarm, respectively.

4. GPHM–SVM-Based Reliability Analysis

The GPHM proposed in this study is employed to efficiently evaluate the ultimate load-carrying capacity F_{L} of steel frame structures. This capacity is taken as the structural system resistance $R(\boldsymbol{X})$ in Eq. (21), where the design external load P is regarded as the load effect S. When the structural ultimate load-carrying capacity F_{L} exceeds the design external load P, the structure is considered safe; otherwise, it is deemed to have failed. Accordingly, the limit-state function for structural system reliability analysis can be established as:

$$G(\boldsymbol{X})=F_{\mathrm{L}}-P\,, \tag{29}$$

In Eq. (29), the ultimate load-carrying capacity F_{L} is influenced by multiple random variables, including the elastic modulus and yield strength of the structural materials, the geometric characteristics of the structure, and loading conditions. The probabilistic properties of these

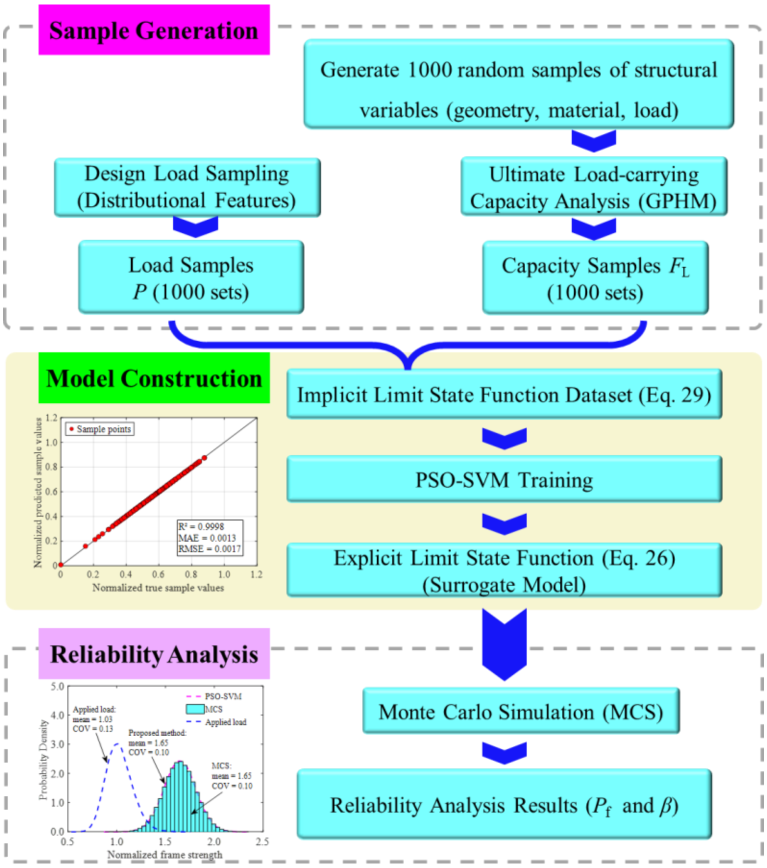

Figure 2. The flowchart of the reliability analysis

variables are directly adopted from the statistical parameters reported in representative benchmark studies available in the literature.

It should be noted that F_L is obtained through a numerical analysis using the proposed GPHM. Therefore, the limit-state function defined in Eq. (29) is implicit in nature. To address this issue, a set of sample data is first generated using the GPHM, and combined with the design load P to construct a limited number of training samples. Subsequently, the SVM is employed to reconstruct the implicit limit-state function in Eq. (29) into explicit form, as expressed in Eq. (26), where the RBF kernel defined in Eq. (25) is adopted.

Based on the reconstructed explicit limit-state function, the MCS is then applied to efficiently perform structural system reliability analysis. The overall analysis procedure is illustrated in Fig. 2.

During the SVM training process, the dataset is divided into training and testing subsets with a ratio of 7:3. Considering that the prediction performance of the SVM is highly sensitive to hyperparameters, the PSO is employed to determine the optimal hyperparameter combination. The search ranges of the SVM hyperparameters and the parameter settings of the PSO are listed in Table 1.

Table 1 The SVM hyperparameter ranges and the PSO parameter settings

Category	Parameter	Description	Value / Range
SVM	C	Penalty parameter	[0.1, 50]
	γ	Insensitive loss parameter	[0.001, 0.1]
	ε	RBF kernel width parameter	[0.1, 10]
PSO	Population size	Number of particles	20
	Maximum iterations	Maximum number of iterations	30
	Dimension	Number of variables	3
	ω	Inertia weight	0.7
	c_1	Cognitive coefficient	1.5
	c_2	Social coefficient	1.5

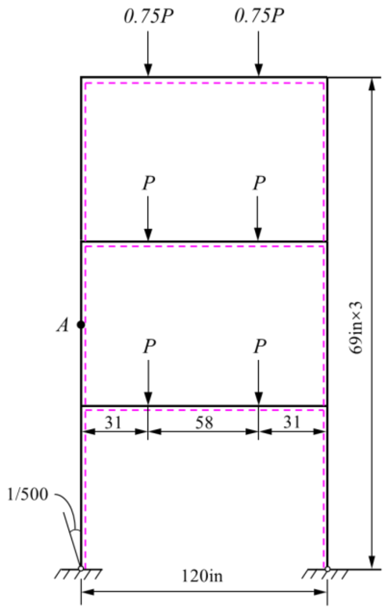

Member	Section	Steel Grade
beam	W6×16	A36
column	W4×13	A441

Figure 3. McNamee's three-story one-bay test steel frame

This study proposes an efficient reliability analysis method for steel frame structural systems by integrating the GPHM and SVM. The GPHM extends the traditional FPHM by considering the combined effects of multiple internal forces on plastic hinge formation, overcoming the limitations of the FPHM and exhibiting substantially higher computational efficiency than the plastic zone-based finite element analysis implemented in Ansys or Abaqus. Although the GPHM is efficient for a single analysis, system reliability analysis still requires a large number of samples, making it difficult to directly combine it with the MCS. To address this issue, the SVM is introduced to reconstruct the implicit limit-state function into an explicit surrogate model using a small number of samples, which can then be combined with the MCS for efficient reliability evaluation. The proposed method fully utilizes the advantages of the GPHM in rapid capacity assessment and the

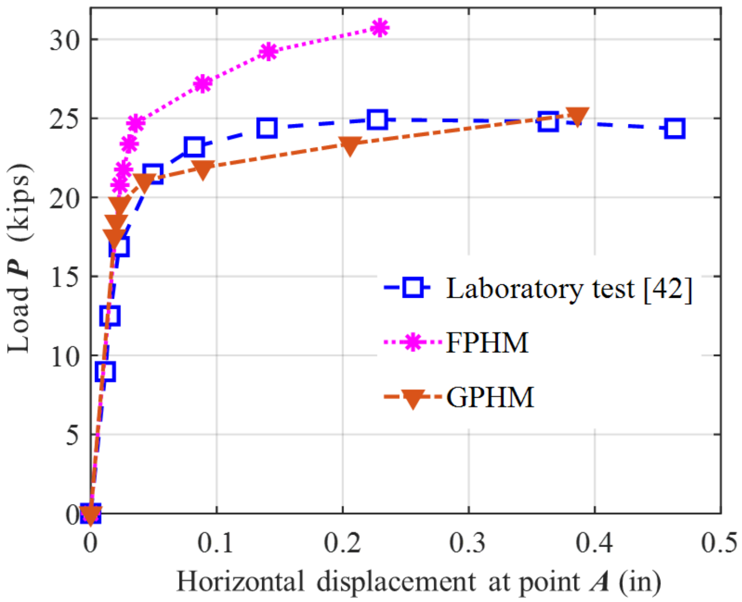

Figure 4. The load-deflection curves for the frame tested by McNamee

SVM in nonlinear approximation with small samples. In addition, the reconstructed explicit function facilitates the calculation of first- and second-order derivatives and can be easily incorporated into the FORM or SORM, further improving computational efficiency.

5. Verification analysis

5.1 McNamee's experimental steel frame

This example, originally tested by McNamee [42] and later investigated by Teh and Clarke [43], is used to study the load-carrying capacity of a three-story, single-bay steel frame. As shown in Fig. 3, the frame is subjected to symmetric vertical concentrated loads without horizontal loading. An initial inclination of 1/500 of the column height is introduced to account for geometric imperfections. The columns are made of A36 W-shaped sections, while the beams are fabricated from A441 steel. The detailed properties are presented in Fig. 3.

Structural failure analysis is performed using both the FPHM and GPHM, and the resulting load–displacement curves are compared with laboratory test, as shown in Fig. 4. The FPHM determines the plastic hinge formation based only on the bending moment, neglecting the axial force, which leads to an overestimation of the ultimate load and a noticeable deviation from the test results. In contrast, the GPHM considers the combined effects of the axial force and bending moment while retaining computational efficiency, resulting in predictions that agree well with the experimental data, especially for the peak load. This demonstrates that the proposed GPHM achieves high accuracy.

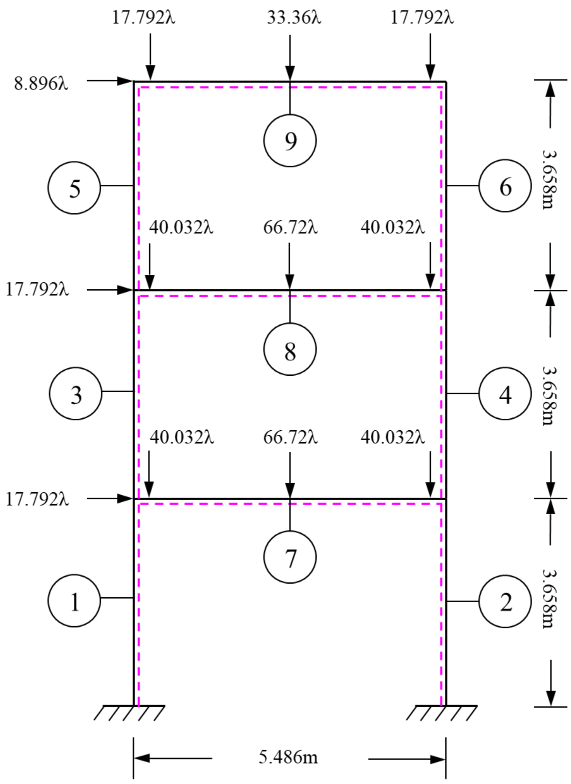

Member	Section
1	W 8x28
2	
3	W 6x25
4	
5	W 6x20
6	
7	W 12x27
8	
9	W 10x21

Figure 5. Frame geometry, member numbering, and initial loading coefficients (units: kN)

5.2 McNamee's experimental steel frame

This example, originally proposed by Cohn and Rafay [17] and later studied by Spiliopoulos and Patsios [19], is used to investigate the effect of axial force on plastic hinge formation. The steel frame, composed of A36 wide-flange sections, is subjected to vertical and horizontal concentrated loads, as shown in Fig. 5. In this study, the ultimate failure analysis of the structure is carried out using both the traditional FPHM and the proposed GPHM to compare the influence of different plastic-hinge determination criteria on the analysis results.

The analysis results of the structural ultimate load-carrying capacity under different sectional plastic hinge formation criteria are summarized in Table 2. As indicated in the table, when the traditional FPHM, in which the formation of plastic hinges is determined solely by the sectional bending moment ($f = m_i = 1$), is adopted, the ultimate load factor reported by Cohn and Rafay [17] is 2.238. In comparison, the ultimate load factor obtained in this study using the self-developed finite element program is 2.246. The close agreement between these two values demonstrates that the proposed analysis program exhibits satisfactory accuracy and reliability in structural modeling as well as in the incremental loading procedure.

Table 2 The structural ultimate load-carrying capacity

method	ultimate load factor λ	Plastic yield criterion of section	Source of result
FPHM	2.238	$f = m_i = 1$	Cohn and Rafay [17]
	2.246	$f = m_i = 1$	Finite element program results (self-developed)
GPHM	1.952	$f = n_i + m_i = 1$	Cohn and Rafay [17]
	2.066	$f = \begin{cases} n_i + \frac{8}{9} m_i = 1\text{, } n_i > 0.2 \\ \frac{1}{2} n_i + m_i = 1\text{, } n_i < 0.2 \end{cases}$	Spiliopoulos and Patsios [19]
	2.037	$\begin{cases} \overline{f} = n_i^4 + 0.2122 n_i^3 m_i + 7.4536 m_i^2 n_i^2 \\ \quad + 0.1813 m_i^3 n_i + m_i^4 \\ r_i^e = \sqrt[4]{\overline{f}} \end{cases}$	Finite element program results (self-developed)
	2.126	$f = n_i^2 + m_i^2 + 3.5 n_i^2 m_i^2 = 1$	Mastan2's result

Meanwhile, Table 2 indicates that when a simple linear generalized yield criterion accounting for both the axial force and bending moment is employed, the ultimate load factor reported by Cohn and Rafay [17] is 1.952, whereas an ultimate load factor of 2.066 is obtained by Spiliopoulos and Patsios [19] using the piecewise linear generalized yield criterion specified in the American steel design codes. These results demonstrate that the axial force has a significant influence on sectional plastic yielding and, consequently, on the ultimate load-carrying capacity of the structure. In contrast, neglecting the axial force and determining the plastic hinge formation based solely on the bending moment in the FPHM leads to a marked overestimation of the structural capacity (2.238 or 2.246).

However, approximating the nonlinear sectional plastic yield surface using a linear generalized yield criterion inevitably introduces approximation errors and limits the attainable accuracy. To overcome these limitations, this study adopts a widely used nonlinear generalized yield criterion and formulates an equivalent homogeneous expression to define the element load-carrying ratio for determining the formation of plastic hinges. Based on this approach, the ultimate load factor is calculated as 2.037, which is in close agreement with the results reported by Spiliopoulos and Patsios [19] (2.066), thereby demonstrating the accuracy and effectiveness of the proposed method.

To further validate the computational accuracy of the proposed GPHM, the steel structural analysis program Mastan2, developed by Ziemian and McGuire [36], is employed. Using the same generalized yield criterion, Mastan2 predicts an ultimate load factor of 2.126, slightly higher than that obtained by the GPHM. This discrepancy arises mainly from the different failure criteria: Mastan2 defines the ultimate state based on the onset of structural unloading, whereas the GPHM identifies it via the global stiffness matrix reaching singularity and the formation of a mechanism. Consequently, a minor deviation in the ultimate load factor is observed between the two methods.

To further compare the two approaches under the same yield criterion, the formation locations of plastic hinges during the loading process, corresponding external loads, and distributions of axial force and bending moment at the ultimate state are analyzed. The results are shown in Figs. 6-7.

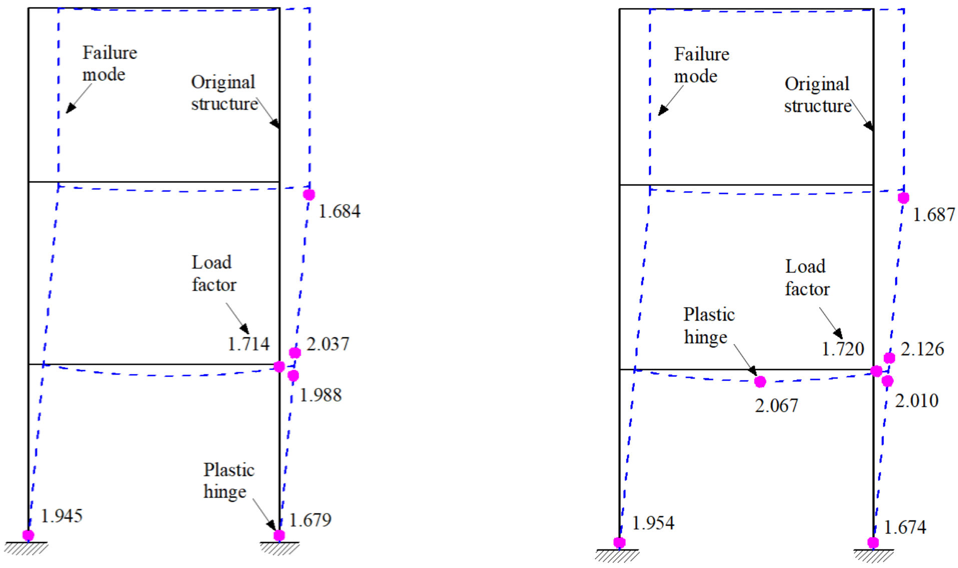

(a) Proposed method (b) Mastan2's result

Figure 6. The formation locations of plastic hinges and corresponding external loads

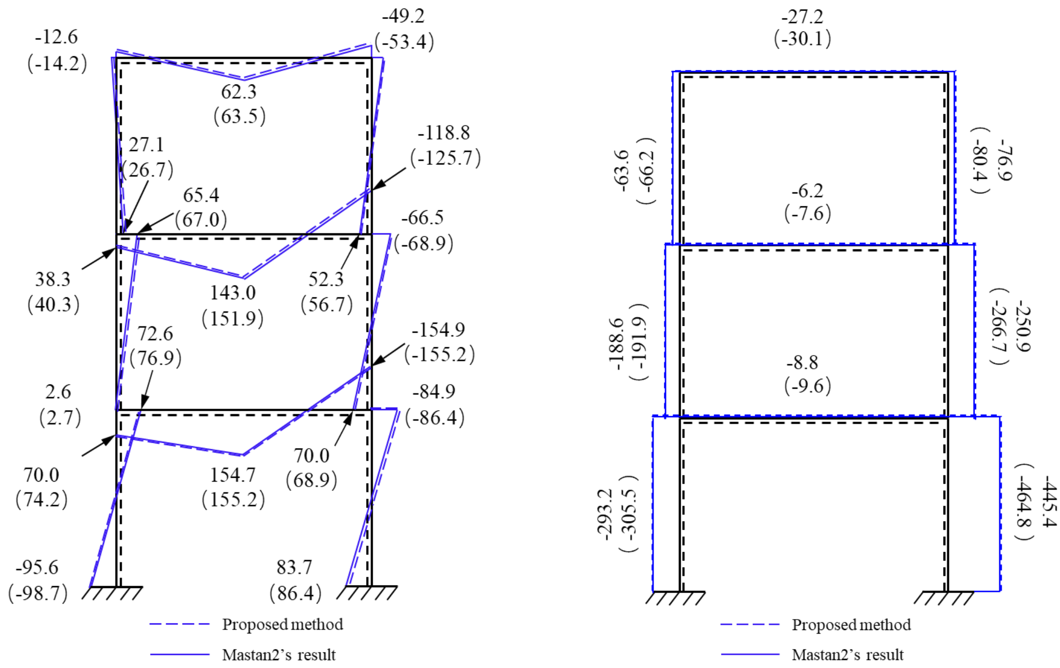

(a) bending moment (Units: kN) (b) axial force (Units: kN/m)

Figure 7. The distributions of axial force and bending moment at the ultimate state

Table 3 The statistical properties of the random variables for function 2

Variable	Distribution	Mean	Standard deviation	Dimension
$x_1 = M_B$	Normal	0.01	0.003	MN·m
$x_2 = D$	Normal	0.30	0.015	m
$x_3 = T_S$	Normal	360	36	MPa
$x_4 = A_S$	Normal	226×10^{-6}	11.3×10^{-6}	m^2
$x_5 = K$	Normal	0.5	0.05	-
$x_6 = B$	Normal	0.12	0.006	m
$x_7 = T_C$	Normal	40	6	MPa

Table 4 Reliability analysis results obtained using different modeling or optimization methods for function 1

Computational content	Literature Results	MCS	PSO-SVM	ANN-SVM	PSO-ANN
reliability indices	2.1891	2.1848	2.1813	2.1710	2.4109
Probability of failure P_F (%)	1.4293 [44]	1.4450	1.4580	1.4966	0.7957
penalty coefficient	—	—	50.0000	26.6747	—
insensitive loss coefficient	—	—	0.0010	0.0085	—
function parameter	—	—	4.0498	1.0740	—

The predicted plastic hinge locations and corresponding external loads during the loading process, obtained using the proposed GPHM and Mastan2, are shown in Fig. 6. The first six plastic hinges are located identically in both methods, and the differences in the associated external loads do not exceed 1%, indicating excellent agreement in simulating the plastic development process. The bending moment and axial force distributions at the ultimate state are presented in Fig. 7(a) and Fig. 7(b), respectively. The comparison demonstrates that the results from the GPHM and Mastan2 closely match, further confirming the high accuracy and reliability of the proposed GPHM in assessing the sectional yielding and predicting the ultimate load-carrying capacity of the structure.

5.3 Reliability analysis of steel frame structural systems

5.3.1 Nonlinear limit-state equations

In this example, two representative limit-state functions widely used in the literature [44-46] are selected to assess the accuracy of the proposed structural reliability analysis method. Function 1, proposed by Lee et al. [44], is used to verify reliability analysis methods for high-dimensional complex structures and involves four independent normally distributed random variables with pronounced nonlinearity. Function 2, adopted by Huang et al. [45], describes the limit state of reinforced concrete beams under pure bending, defined as the difference between the ultimate and

Table 5 Reliability analysis results obtained using different modeling or optimization methods for function 2

Computational content	Literature Results	MCS	PSO-SVM	ANN-SVM	PSO-ANN
reliability indices	3.3991	3.3975	3.4024	3.4057	3.5019
Probability of failure P_F (%)	3.38×10^{-2} [45]	3.40×10^{-2}	3.34×10^{-2}	3.30×10^{-2}	2.31×10^{-2}
penalty coefficient	—	—	40.0523	8.0452	—
insensitive loss coefficient	—	—	0.0013	0.0014	—
function parameter	—	—	1.5165	4.3891	—

actual sectional bending moments. The statistical properties of the random variables are listed in Table 3.

$$\textit{Function } 1:\ G(\boldsymbol{X}) = -x_1^2 - x_2^2 - x_3^2 - x_4^2 + 10x_1 + 12x_2 + 12x_3 + 12x_4 - 43\ ,$$

$$x_i \sim N(0,\ 1)\ ,\ i = 1 \sim 4$$

$$\textit{Function } 2:\ G(\boldsymbol{X}) = \left(1 - x_5 \frac{x_4 x_3}{x_6 x_2 x_7}\right) x_4 x_2 x_3 - x_1$$

For these two functions, 1000 sets of random samples are generated and normalized. Subsequently, different machine learning models and hyperparameter optimization methods are employed to predict the structural failure probability and corresponding reliability index. The results are compared with those reported in the literature as well as with the MCS results, as presented in Tables 4 and 5. Specifically, the PSO-SVM denotes the use of the PSO to search for the optimal hyperparameters of the SVM for reconstructing the limit-state function; the ANN-SVM employs the use of the ANN to optimize the SVM hyperparameters; and the PSO-ANN utilizes the use of the PSO to optimize the hyperparameters of the ANN model.

For Function 1 (see Table 4), the PSO-SVM method yields a reliability index of 2.1813 and a failure probability of 1.4580%, showing excellent agreement with the MCS results (2.1848 / 1.4450%) and the literature values reported in [44] (2.1891 / 1.4293%). The primary distinction between the PSO-SVM and ANN-SVM lies in their hyperparameter optimization strategies: the former employs the PSO for global search, whereas the latter relies on the ANN-based prediction. Owing to the sensitivity of the ANN to initial weights, sample size, and network architecture, its optimization process may exhibit slight variability, resulting in marginally less accurate predictions (2.1710 / 1.4966%) compared to the PSO-SVM.

A further comparison between the PSO-SVM and PSO-ANN indicates that, although both methods employ the PSO for hyperparameter optimization, they differ in the underlying surrogate models. In civil engineering applications involving high-fidelity numerical simulations—such as the ultimate load-carrying capacity of steel frames or the mechanical response of reinforced concrete structures—the generation of training samples typically depends on computationally intensive finite element analyses, making large-scale data acquisition challenging in practice. Therefore, only 1000 samples are generated in this study, which is consistent with realistic engineering conditions. Under such small-sample circumstances, the SVM may exhibit superior generalization performance compared to the ANN, thereby leading to the slightly lower accuracy of the PSO-ANN relative to the PSO-SVM.

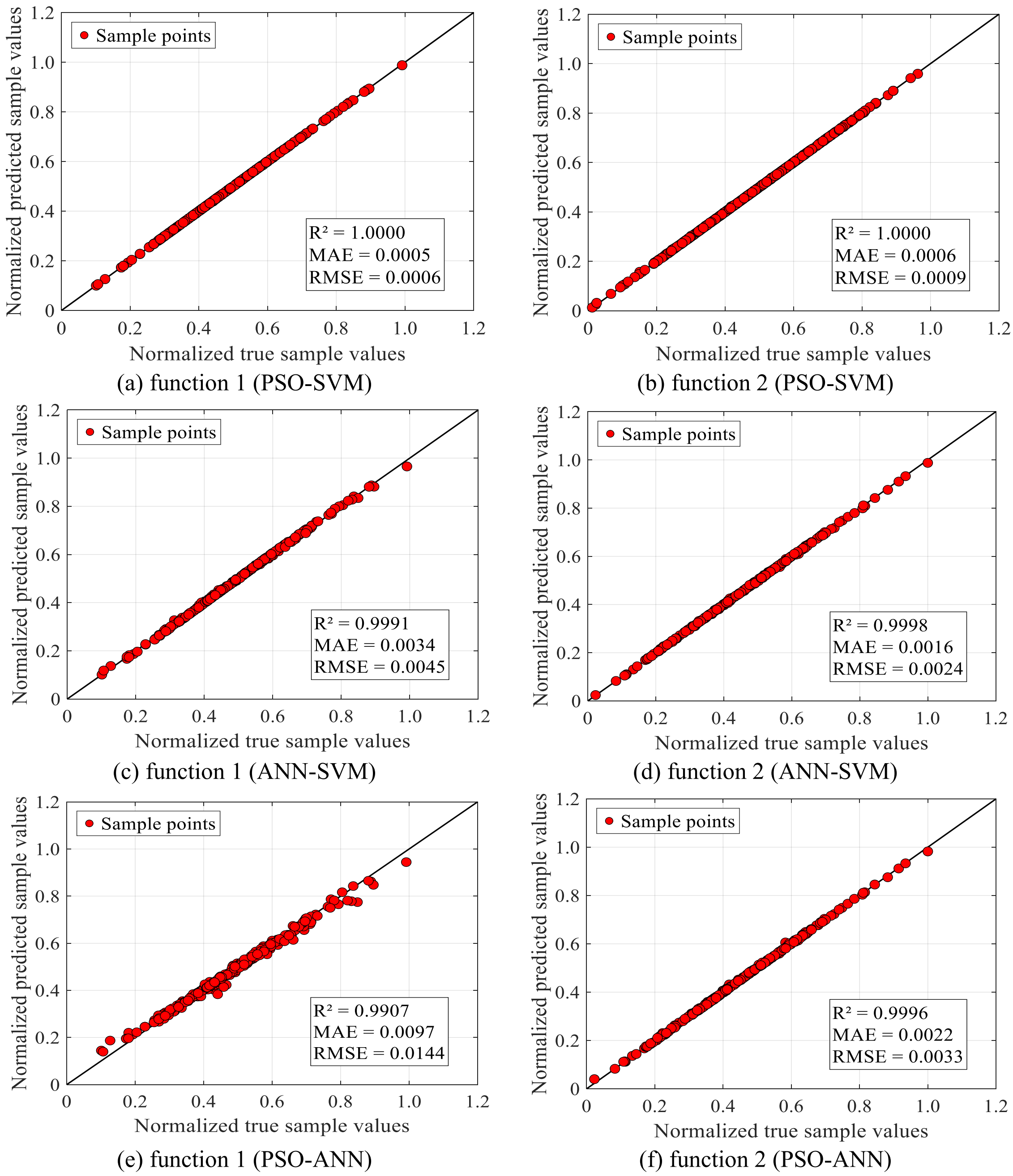

Figure 8. The prediction performance of different methods

A similar trend is observed for Function 2 (see Table 5). The PSO-SVM yields a reliability index of 3.4024 and a corresponding failure probability of $3.34 \times 10^{-2}\%$, which agree closely with the MCS results (3.3975 / $3.40\times10^{-2}\%$) and the literature values reported in [45] (3.3991 / $3.38\times10^{-2}\%$). The ANN-SVM and PSO-ANN produce reliability indices of 3.4057 and 3.5019,

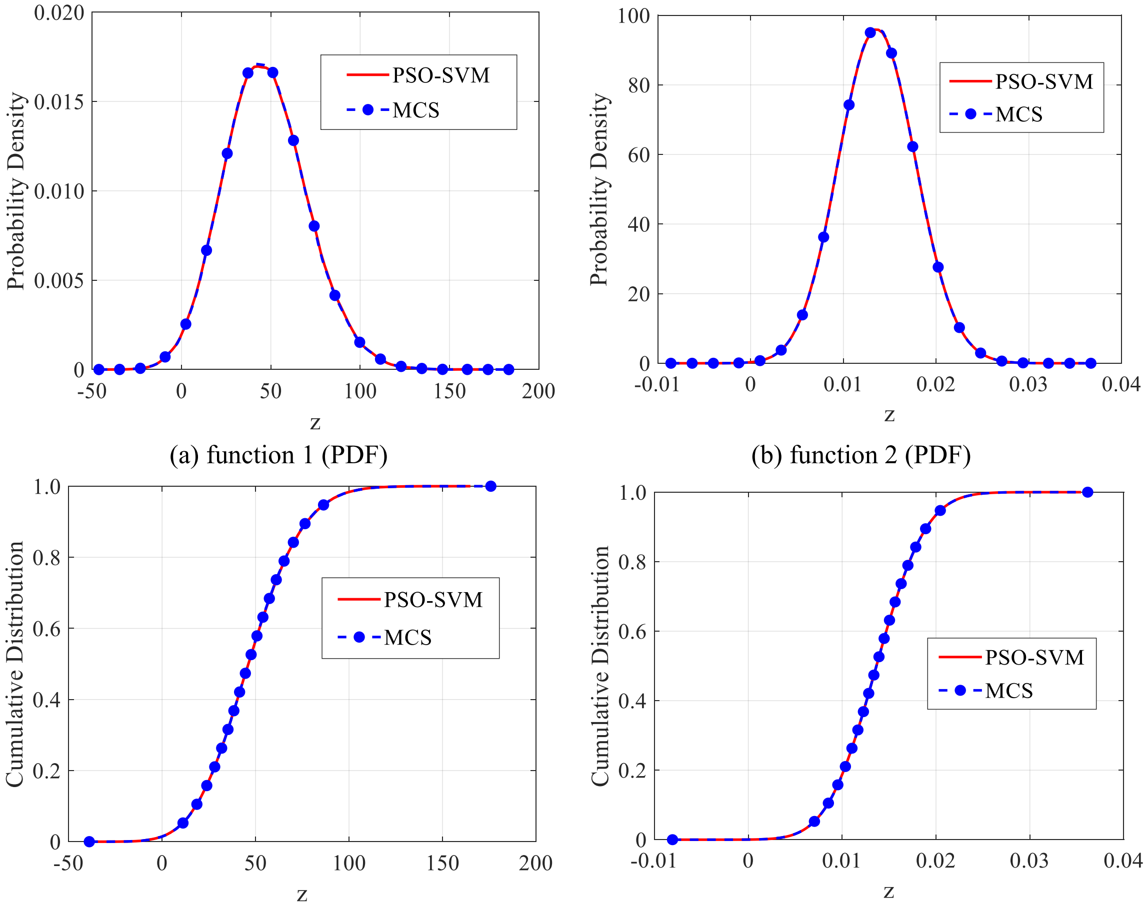

(a) function 1 (PDF) (b) function 2 (PDF)

(c) function 1 (CDF) (d) function 2 (CDF)

Figure 9. The probability distributions of different methods

respectively, exhibiting only minor discrepancies among the different approaches and further confirming the effectiveness of the PSO-SVM under small-sample conditions.

In addition, the penalty coefficient, ε-insensitive loss parameter, and kernel parameters optimized by the PSO and ANN are summarized in Tables 4 and 5, ensuring the reproducibility and robustness of the SVM models.

To further investigate the accuracy and applicability of different limit-state function reconstruction methods, the predictive performance of the PSO-SVM, the ANN-SVM, and the

PSO-ANN is illustrated in Fig. 8 through scatter plots of normalized predicted values versus normalized true values.

For Function 1 (Fig. 8(a), 8(c), and 8(e)), the predicted points of all three methods are closely clustered around the 1:1 reference line, demonstrating excellent fitting accuracy and strong generalization capability. Among the models, the PSO-SVM exhibits the highest performance, with R^2 = 1.0000, MAE = 0.0005, and RMSE = 0.0006. The ANN-SVM achieves slightly lower accuracy (R^2 = 0.9991, MAE = 0.0034, RMSE = 0.0045), while the PSO-ANN shows relatively lower performance (R^2 = 0.9907, MAE = 0.0097, RMSE = 0.0144).

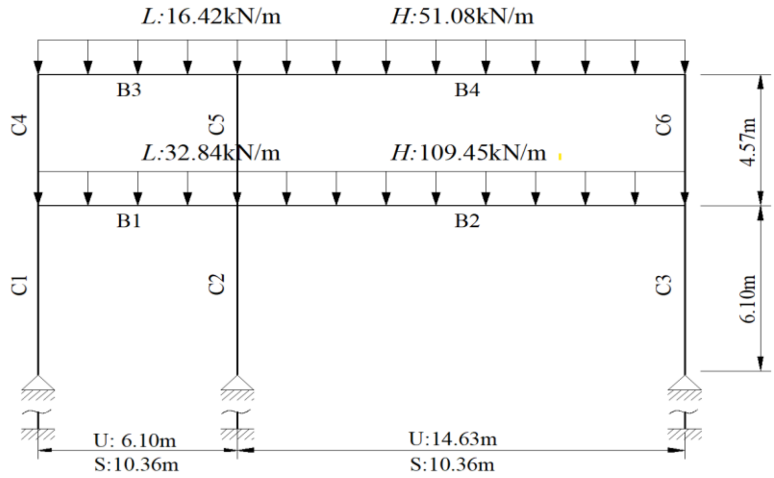

(a) Dimensions and loads of frames

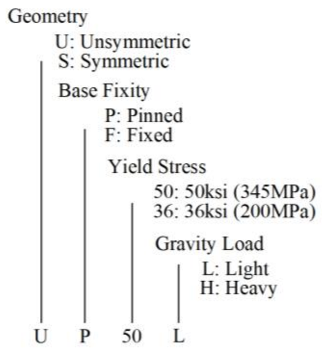

(b) Frame nomenclature

Figure 10. Loads and dimensions of Ziemian's frames

A similar trend is observed for Function 2 (Fig. 8(b), 8(d), and 8(f)), further demonstrating the superior predictive performance of the PSO-SVM. This can be attributed to the differences in hyperparameter optimization strategies: the PSO-SVM employs a global search, which improves stability and robustness, whereas the ANN-SVM is more sensitive to initialization, sample size, and network configuration. Under the limited sample size used in this study, the SVM generally exhibits better generalization than the ANN, accounting for the slightly lower accuracy of the PSO-ANN compared to the PSO-SVM.

Overall, the PSO-SVM demonstrates superior prediction accuracy, stability, and robustness under limited-data conditions. Therefore, it is adopted in the subsequent analysis to reconstruct the structural limit-state function and perform reliability assessment.

The probability density functions (PDFs) and cumulative distribution functions (CDFs) of the two nonlinear limit-state functions, obtained by the PSO-SVM and MCS, are presented in Fig. 9. As shown in Fig. 9(a) and 9(b), the PDFs from the PSO-SVM closely match those from the MCS in terms of the peak position, spread, and tail behavior, indicating that the PSO-SVM accurately

Table 6 The cross-section dimensions of representative frames

Frame	UP36H	UP50H	SP36L	SP50H
C1	W8 × 15	W12 × 14	W14 × 61	W14 × 53
C2	W14 × 132	W14 × 99	W14 × 132	W14 × 74
C3	W14 × 120	W14 × 82	W14 × 61	W14 × 53
C4	W8 × 13	W10 ×12	W12 × 14	W14 × 53
C5	W14 × 120	W14 × 109	W14 × 22	W12 × 19
C6	W14 × 109	W14 × 109	W12 × 14	W14 × 53
B1	W27 × 84	W27 × 84	W24 × 55	W27 × 84
B2	W36 × 170	W36 × 135	W24 × 55	W27 × 84
B3	W21 × 44	W18 × 40	W16 × 31	W24 × 55
B4	W27 × 102	W27 × 94	W16 × 31	W24 × 55

Table 7 The statistical characteristics of random variables

Variable	Distribution	Mean	Standard deviation
External load (Q)	Lognormal	1.026	0.132
Material yield strength (f_y)	Normal	1.05	0.1
Member cross-section area (A)	Normal	0.993	0.034
Elastic modulus (E)	Normal	1.025	0.0324

captures the probabilistic characteristics of the structural response. The corresponding CDFs, shown in Fig. 9(c) and 9(d), also exhibit excellent agreement between the two methods across both the central and tail regions, which is particularly important for reliability assessment. These results further confirm the accuracy, consistency, and robustness of the proposed PSO-SVM approach for structural reliability analyses.

5.3.2 Reliability analysis of steel frame structural systems

The steel frame structures analyzed in this section are based on the classical model proposed by Ziemian [47], which represents a typical low-rise industrial building. Subsequently, Buonopane and Schafer [48] conducted a series of system reliability analyses on these steel frame structures. The geometry, boundary conditions, and external loading of the 16 frames are shown in Fig. 10(a), and the naming scheme of these frames is illustrated in Fig. 10(b). Table 6 lists the sectional dimensions of four representative frames—UP36H, UP50H, SP36L, and SP50H—while the remaining 12 frames follow the original settings in Ziemian [47]. In the reliability analysis, the external loads, member yield strength, sectional dimensions, and material elastic modulus are all treated as random variables, and their statistical properties are presented in Table 7. To enhance the numerical stability, symmetric frames are assigned a small initial lateral imperfection equal to 1/500 of the structural height, whereas no initial imperfections are introduced for asymmetric frames. Subsequently, the failure probability and reliability index of the steel frame are evaluated.

In the reliability analysis of the steel frames, 1000 samples of the structural ultimate load-carrying capacity are first generated using the proposed GPHM and subsequently normalized. The

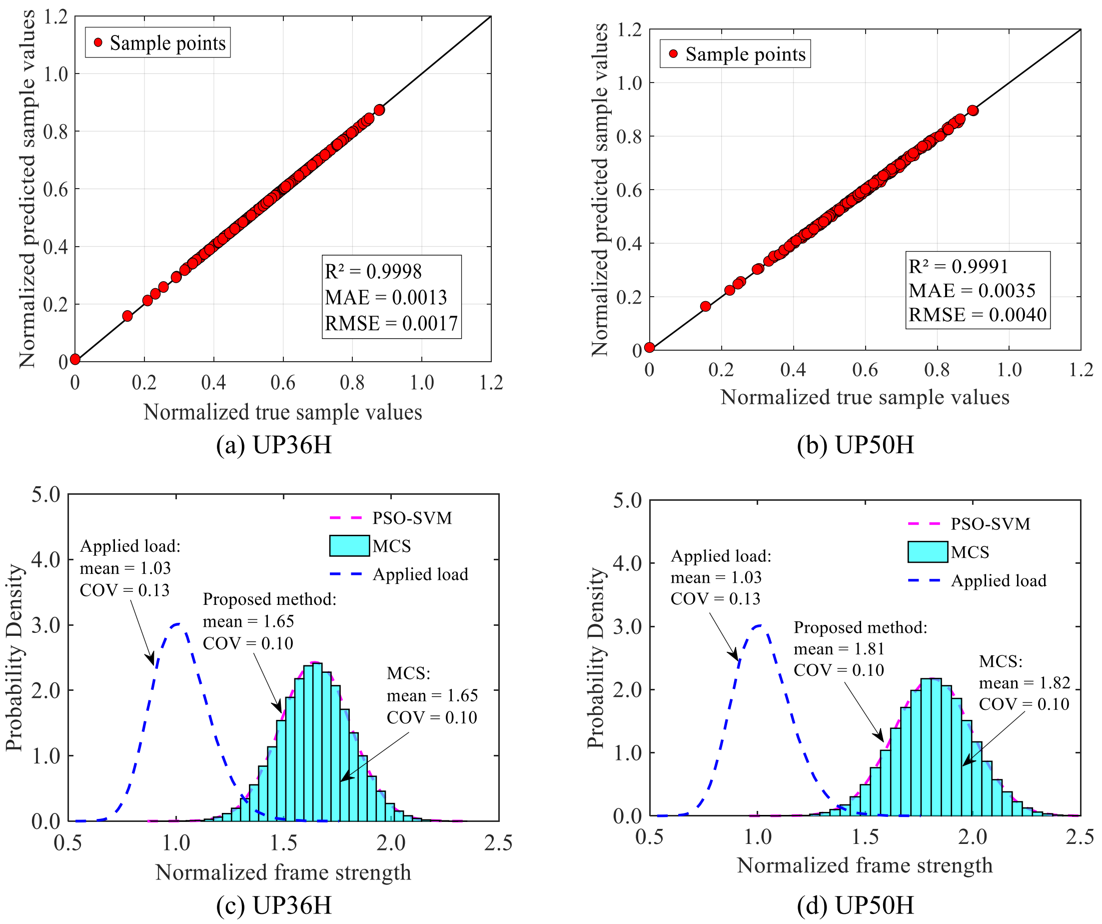

Figure 11. The predictions of different analysis methods and probability density functions at the structural limit state

PSO algorithm is then employed to determine the optimal hyperparameters of the SVM model, which is used to reconstruct the limit-state function for reliability analysis. The structural failure probability and reliability index are evaluated based on the SVM-based reconstructed function. For validation, the MCS with 100,000 samples is used for comparison.

The prediction performance and resulting strength probability distributions for the two representative frames, UP36H and UP50H, are presented in Fig. 11. The scatter plots comparing the normalized values predicted by the SVM model with the normalized true values obtained from the proposed GPHM are shown in Fig. 11(a) and Fig. 11(b). In both frames, the sample points cluster tightly around the 1:1 reference line, demonstrating that the SVM-based reconstructed limit-state equations provide excellent fitting and generalization performance. The coefficients of determination are $R^2 = 0.9998$ for UP36H and $R^2 = 0.9991$ for UP50H, with very small MAE and RMSE values, further confirming the high prediction accuracy of the SVM-based reconstructed limit-state functions.

Table 8 Frame reliability and corresponding parameters of the strength distributions

Frame	PSO-SVM				MCS			
	$P_F\,(\times 10^{-3})$	β	Mean	COV	$P_F\,(\times 10^{-3})$	β	Mean	COV
UP36L	3.36	2.71	1.63	0.10	3.38	2.71	1.63	0.10
UP36H	2.53	2.80	1.65	0.10	2.82	2.77	1.65	0.10
UF36L	3.88	2.66	1.61	0.10	4.08	2.65	1.61	0.10
UF36H	3.58	2.69	1.62	0.10	3.64	2.68	1.62	0.10
UP50L	2.43	2.81	1.65	0.10	2.63	2.79	1.65	0.10
UP50H	0.46	3.31	1.81	0.10	0.51	3.29	1.82	0.10
UF50L	3.98	2.65	1.61	0.10	3.92	2.66	1.61	0.10
UF50H	0.33	3.41	1.84	0.10	0.39	3.36	1.84	0.10
SP36L	1.33	3.00	1.72	0.10	1.37	2.99	1.72	0.10
SP36H	2.29	2.84	1.67	0.10	2.36	2.83	1.67	0.10
SF36L	3.79	2.67	1.61	0.10	3.90	2.66	1.61	0.10
SF36H	20.85	2.03	1.43	0.10	22.54	2.01	1.44	0.10
SP50L	2.49	2.81	1.64	0.10	3.03	2.75	1.64	0.10
SP50H	2.94	2.75	1.63	0.10	3.49	2.70	1.63	0.10
SF50L	12.11	2.25	1.49	0.10	13.39	2.21	1.49	0.10
SF50H	1.82	2.90	1.68	0.10	2.21	2.85	1.68	0.10

The probability density functions (PDFs) of the structural ultimate load-carrying capacity predicted by the SVM-based reconstructed limit-state functions are compared with those obtained from the MCS in Fig. 11(c) and Fig. 11(d), which also show the PDF of the applied external load. The distribution curves of the reconstructed function closely match the MCS results, with nearly identical mean values and coefficients of variation (UP36H: mean ≈ 1.65, COV = 0.10; UP50H: mean ≈ 1.81-1.82, COV = 0.10), further confirming the high predictive accuracy of the SVM-based reconstructed limit-state functions. A comparison of Fig. 11(c) and Fig. 11(d) also illustrates the relationship between the structural ultimate capacity and the applied external load. The two distributions overlap very slighttly, indicating that the frame structures exhibit a high level of reliability.

To further quantify the reliability of the steel frames, Table 8 summarizes the failure probability, reliability index, mean and coefficient of variation (COV) of the structural ultimate load-carrying capacity. For comparison, the corresponding results from the MCS are also provided. In the proposed approach, 1,000 structural ultimate load-carrying capacity samples are first analyzed using the proposed GPHM and then used to reconstruct the limit-state function via the SVM for reliability evaluation, whereas the MCS uses 100,000 GPHM-analyzed samples to assess structural reliability.

The results show that both methods yield highly consistent failure probabilities, reliability indices, mean capacities, and COVs. The deviations between the proposed method and the MCS are small for all frames, and the reliability indices are nearly identical. These results demonstrate that the structural reliability analysis framework developed in this study—namely, efficiently generating samples of structural ultimate load-carrying capacity using the proposed GPHM, reconstructing the limit-state function via the SVM, and then performing reliability analysis—can provide accurate and reliable evaluations across different structural configurations and strength levels. Table 6 also indicates that high-strength frames (e.g., UP50H and UF50H) have significantly higher load-carrying capacities and lower failure probabilities than low-strength frames, whereas the COV remains at 0.10 for all frames, reflecting the uniform treatment of material and geometric randomness.

6. Conclusions

This study proposes a generalized plastic-hinge method (GPHM) for efficient evaluation of the ultimate load-carrying capacity of steel frame structures. This method introduces an element load-carrying ratio that accounts for the combined effects of the sectional axial force and bending moment. This ratio replaces the nondimensional sectional bending moment in the traditional FPHM for determining the plastic hinge formation. Furthermore, the structural ultimate load-carrying capacity samples generated by the proposed GPHM are used to reconstruct the limit-state function using the SVM model. This enables the system-level reliability analysis of steel frame structures. The main conclusions are as follows:

(1) The traditional FPHM exploits the proportional scaling property between linearly elastic sectional internal forces and external loads, allowing the efficient identification of plastic hinges and tracking of the structural failure path. However, because it adopts only the bending moment as the criterion for plastic hinge formation, it overestimates the ultimate load-carrying capacity of steel frame structures.

(2) The proposed GPHM defines an element load-carrying ratio using an equivalent homogeneous function of the generalized yield criterion, thereby capturing the combined effects of the axial force and bending moment on plastic hinge formation. This ratio retains the proportional scaling property with external loads from the traditional FPHM, allowing the GPHM to maintain high computational efficiency while significantly improving the accuracy, effectively overcoming the limitations of the traditional FPHM.

(3) Using the proposed GPHM, a small set of structural ultimate load-carrying capacity samples is generated, and the PSO is applied to determine the optimal SVM hyperparameters. This allows accurate reconstruction of the limit-state equation with few samples, reducing the reliance on large datasets for reliability analysis.

(4) The system-level reliability analysis results of steel frame structures based on the SVM-based reconstructed limit-state function closely match those from the MCS, which verifies the superiority of the proposed method in terms of computational accuracy and efficiency for structural reliability analysis.

(5) The proposed GPHM is currently primarily applicable to planar steel frame structures. Future work will focus on extending it to three-dimensional structural systems and higher-dimensional stochastic spaces, as well as deriving the first- and second-order derivatives of the explicit limit-state function reconstructed via the SVM, thereby enabling efficient integration with the FORM and SORM to further improve the computational efficiency of structural reliability analysis.

Acknowledgements

The financial support provided by the Chongzuo City Science and Technology Plan (Grant Nos. 2024ZC018473 and 2024ZC017960) is greatly acknowledged.

References

1. Chen, W. F. (2012). Structural stability: From theory to practice. Engineering Structures, 22(2), 116-122. https://doi.org/10.1016/S0141-0296(98)00100-X.
2. Iu, C. K., Chen, W. F., Chan, S. L., Ma, T. W. (2008). Direct second-order elastic analysis for steel frame design. KSCE Journal of Civil Engineering, 12(6), 379-389. https://doi.org/10.1007/s12205-008-0379-3.
3. Liu, W., Zhang, B., Shen, C., Li, Y. C. (2022). Stability analysis for spatial autoparametric resonances of framed structures. International Journal of Structural Stability and Dynamics, 22(6), 2250065. https://doi.org/10.1142/S0219455422500651.
4. Alvarenga, A. R. (2020). Plastic-zone advanced analysis - formulation including semi-rigid connection. Engineering Structures, 212, 110435. https://doi.org/10.1016/j.engstruct.2020.110435.
5. Nguyen, P. C., Le-Van, B., Thanh, S. D. T. V. (2020). Nonlinear inelastic analysis of 2D steel frames: An improvement of the plastic hinge method. Engineering, Technology & Applied Science Research, 10(4): 5974-5978. https://doi.org/10.48084/etasr.3600.
6. Ngo-Huu, C., Kim, S. (2009). Practical advanced analysis of space steel frames using fiber hinge method. Thin Walled Structures, 47(4), 421-430. https://doi.org/10.1016/j.tws.2008.08.007.
7. Liew, J. Y. R., White, D. W., Chen, W. F. (1993). Second-order refined plastic-hinge analysis for frame design. Part I. Journal of Structural Engineering, 119(11), 3196-3216. https://doi.org/10.1061/(ASCE)0733-9445(1993)119:11(3196).
8. Liew, J. Y. R., White, D. W., Chen, W. F. (1993). Second-order refined plastic-hinge analysis for frame design. Part II. Journal of Structural Engineering, 119(11), 3217-3237. https://doi.org/10.1061/(ASCE)0733-9445(1993)119:11(3217).
9. Tang, Y. Q., Zhu, H., Du, E. F. (2022). A novel incremental iterative force recovery method for second-order beam-column elements in plastic hinge analysis of steel frames. International Journal of Structural Stability and Dynamics, 22(2), 2250027. https://doi.org/10.1142/S0219455422500274.
10. Thai, H. T., Kim, S. E., Kim, J. (2017). Improved refined plastic hinge analysis accounting for local buckling and lateral-torsional buckling. Steel and Composite Structures, 24(3), 339-349. https://doi.org/10.12989/scs.2017.24.3.339.
11. Lemes, Í. J. M., Silveira, R. A. M., Silva, A. R. D., Rocha, P. A. S. (2017). Nonlinear analysis of two-dimensional steel, reinforced concrete and composite steel-concrete structures via coupling SCM/RPHM. Engineering Structures, 147, 12-26. https://doi.org/10.1016/j.engstruct.2017.05.042.
12. Rahman, M. K. (1998). Ultimate strength estimation of ships' transverse frames by incremental elastic-plastic finite element analysis. Marine Structures, 11(7), 291-317. https://doi.org/10.1016/S0951-8339(98)00019-7.
13. Wang, C. K. (1963). General computer program for limit analysis. Journal of the Structural Division, ASCE, 89(6), 101-117. https://doi.org/10.1061/JSDEAG.0000994.
14. Wong, M. B., Loi, F. T. (1987). Yield surface linearization in elastoplastic analysis. Computers & structures, 26(6): 951-956. https://doi.org/10.1016/0045-7949(87)90112-X.
15. Yang, L. F., Liu, J. M., Yu, B., Ju, J. W. (2017). Failure path-independent methodology for structural damage evolution and failure mode analysis of framed structures. International Journal of Damage Mechanics, 26(2), 274-292. https://doi.org/10.1177/1056789516662626.
16. Bott, B. A. (1966). Elastic-plastic analysis of frames including axial force effect on moment capacity. Fritz Engineering Laboratory Report No. 297.21, Lehigh University, Bethlehem, USA.

17. Cohn, M. Z., Rafay, T. (1974). Collapse load analysis of frames considering axial forces. Journal of the Engineering Mechanics Division, 100(4), 773-794. https://doi.org/10.1061/JMCEA3.0001919.
18. Uslu, F., Bayer, M. T., Saraçoğlu, M. H. (2021). New elastoplastic analysis of two-dimensional frames when some plastic hinges unload elastically. International Journal of Steel Structures, 21(2), 525-538. https://doi.org/10.1007/s13296-021-00453-6.
19. Spiliopoulos, K. V., Patsios, T. N. (2010). An efficient mathematical programming method for the elastoplastic analysis of frames. Engineering Structures, 32(5), 1199-1214. https://doi.org/10.1016/j.engstruct.2009.12.045.
20. Yu, B., Ning, C., Li, B. (2017). Probabilistic durability assessment of concrete structures in marine environments: Reliability and sensitivity analysis. China Ocean Engineering, 31(1): 63-73. https://doi.org/10.1007/s13344-017-0008-3.
21. Taiwo, R., Ben Seghier, M. E. A., Zayed, T. (2023). Toward sustainable water infrastructure: the state-of-the-art for modeling the failure probability of water pipes. Water Resources Research, 59(4), e2022WR033256. https://doi.org/10.1029/2022WR033256.
22. Zhao, Y. G., Ono, T. (1999). A general procedure for first/second-order reliabilitymethod (FORM/SORM). Structural safety, 21(2), 95-112. https://doi.org/10.1016/S0167-4730(99)00008-9.
23. Hu, Z., Mansour, R., Olsson, M., Du, X. (2021). Second-order reliability methods: a review and comparative study. Structural and multidisciplinary optimization, 64: 3233-3263. https://doi.org/10.1007/s00158-021-03013-y.
24. Tawfik, M. E., Bishay, P. L., Sadek, E. A. (2018). Neural network-based second order reliability method (NNBSORM) for laminated composite plates in free vibration. Computer Modeling in Engineering & Sciences, 115(1), 105. https://doi.org/10.3970/cmes.2018.115.105.
25. Asgarkhani, N., Kazemi, F., Jankowski, R., Formisano, A. (2025). Dynamic ensemble-learning model for seismic risk assessment of masonry infilled steel structures incorporating soil-foundation-structure interaction. Reliability Engineering & System Safety, 267(A) : 111839. https://doi.org/10.1016/j.ress.2025.111839.
26. Feng, B., Zhou, X. P. (2025). The novel physics-enhanced graph neural network for phase-field fracture modelling. Computer Methods in Applied Mechanics and Engineering, 446, 118284. https://doi.org/10.1016/j.cma.2025.118284.
27. Ma, J. X., Zhou, X. P. (2025). A minimum potential energy-based nonlocal physics-informed deep learning method for solid mechanics. Journal of Applied Mechanics, 92(3): 031008. https://doi.org/10.1115/1.4067594.
28. Feng, K., Zhou, X. P. (2026). A Graph Networks-Based Plastic Fracture Surrogate Model for Geomaterials. International Journal for Numerical Methods in Engineering, 127(2), e70266. https://doi.org/10.1002/nme.70266.
29. Li, H., Lü, Z., Yue, Z. (2006). Support vector machine for structural reliability analysis. Applied Mathematics and Mechanics, 27(10): 1295-1303. https://doi.org/10.1007/s10483-006-1001-z.
30. Keshtegar, B., Seghier, M. E. A. B., Zio, E., Correia, J. A. F. O., Zhu, S. P., Trung, N. T. (2021). Novel efficient method for structural reliability analysis using hybrid nonlinear conjugate map-based support vector regression. Computer Methods in Applied Mechanics and Engineering, 381, 113818. https://doi.org/10.1016/j.cma.2021.113818.
31. Shi, Z., Lu, Z., Zhang, X., Li, L. (2021). A novel adaptive support vector machine method for reliability analysis. Proceedings of the Institution of Mechanical Engineers, Part O: Journal of Risk and Reliability, 235(5): 896-908. https://doi.org/10.1177/1748006X211003371.
32. Asgarkhani, N., Kazemi, F., Jankowski, R. (2023). Machine learning-based prediction of residual drift and seismic risk assessment of steel moment-resisting frames considering soil-structure interaction. Computers & Structures, 289, 107181. https://doi.org/10.1016/j.compstruc.2023.107181.
33. Asgarkhani, N., Kazemi, F., Jankowski, R. (2025). Machine-learning based tool for seismic response assessment of steel structures including masonry infill walls and soil-foundation-structure interaction. Computers & Structures, 317, 107918. https://doi.org/10.1016/j.compstruc.2025.107918.

34. Yang, L. F., Yang, D. W. (2017). Ultimate bearing capacities analysis of frame structures based on accumulated load effects. Chinese Journal of Applied Mechanics, 34(2), 210-215+398. https://10.11776/cjam.34.02.B034. [In Chinese]
35. McGuire, W., Gallagher, R. H., Ziemian, R. D. (2000). Matrix structural analysis. Createspace Independent Publishing Platform, Scotts Valley, CA, USA.
36. Ziemian, R. D., McGuire, W. (2024). Structural analysis software-mastan2 v5.2.2. (Available from www.mastan2.com)
37. Duan, L., Chen, W. F. (1990). A yield surface equation for doubly symmetrical sections. Engineering Structures, 12(2), 114-119. https://doi.org/10.1016/0141-0296(90)90016-L.
38. Yang, L. F., Li, Q., Zhang, W., Wu, W. L., Lin, Y. H. (2014). Homogeneous generalized yield criterion based elastic modulus reduction method for limit analysis of thin-walled structures with angle steel. Thin-Walled Structures, 80, 153-158. https://doi.org/10.1016/j.tws.2014.02.030.
39. Wu, K., Zhou, S. H., Li, Q., Xu, L. L., Yu, L., Xu, Y. Zhang, Y. R., Yang, Z. H. (2024). A robust approach for bond strength prediction of mortar using machine learning with SHAP interpretability. Materials Today Communications, 41, 110667. https://doi.org/10.1016/j.mtcomm.2024.110667.
40. Elgeldawi, E., Sayed, A., Galal, A. R., Zaki, A. M. (2021). Hyperparameter tuning for machine learning algorithms used for arabic sentiment analysis. Informatics, 8(4), 79. https://doi.org/10.3390/informatics8040079.
41. Ghosh, G., Mandal, P., Mondal, S. C. (2019). Modeling and optimization of surface roughness in keyway milling using ANN, genetic algorithm, and particle swarm optimization. The International Journal of Advanced Manufacturing Technology, 100, 1223-1242. https://doi.org/10.1007/s00170-017-1417-4.
42. McNamee, B. M., Lu, L. W. (1972). Inelastic multistory frame buckling. Journal of the Structural Division, 98(7), 1613-1631. https://doi.org/10.1061/JSDEAG.0003284.
43. Teh, L. H., Clarke, M. J. (1999). Plastic-zone analysis of 3D steel frames using beam elements. Journal of structural engineering, 125(11), 1328-1337. https://doi.org/10.1061/(ASCE)0733-9445(1999)125:11(1328)
44. Lee, I., Noh, Y., Yoo, D. (2012). A novel second-order reliability method (SORM) using noncentral or generalized chi-squared distributions. Journal of Mechanical Design, 134(10), 100912. https://doi.org/10.1115/DETC2012-70276.
45. Huang, X., Li, Y., Zhang, Y., Zhang, X. (2018) A new direct second-order reliability analysis method. Applied Mathematical Modelling, 55, 68-80. https://doi.org/10.1016/j.apm.2017.10.026.
46. Mansour, R., Olsson, M. (2014). A closed-form second-order reliability method using noncentral chi-squared distributions. Journal of Mechanical Design, 136(10), 101402. https://doi.org/10.1115/1.4027982.
47. Ziemian, R. D. (1990). Advanced methods of inelastic analysis in the limit states design of steel structures. Ph.D. Dissertation, Cornell University, Ithaca.
48. Buonopane, S. G., Schafer, B. W. (2006). Reliability of steel frames designed with advanced analysis. Journal of Structural Engineering, 132(2), 267-276. https://doi.org/10.1061/(ASCE)0733-9445(2006)132:2(267).